Benchmark study of numerical solvers for the prediction of interior noise transmission excited by A-pillar vortex

Munhwan CHO[1]; Hyoung Gun KIM[2]; Chisung OH[3]; Kang Duck IH[4]

Ashok KHONDGE[5]; Fred MENDONÇA[6]; Jongyun LIM[7];

Eui-Sung CHOI[8]; Bastien GANTY[9]; Raphael HALLEZ[10]

[1-4] Hyundai Motor Group, Korea

[5] ANSYS Inc., India

[6] CD-adapco, UK

[7] ESI Korea, Korea

[8] Exa Korea Inc., Korea

[9] Free Field Technology, Belgium

[10] Siemens PLM, Belgium

ABSTRACT

Wind noise in road vehicles is being made much quieter to satisfy customers' demands for comfortable driving environments. The interaction between outside flows and exterior surfaces at the front and sides of a vehicle forms a strong swirling fluid structure called A-pillar vortex which is one of the most crucial wind noise sources. The geometrical characteristics of the A-pillar can determine the size or strength of the vortex structure. It is tremendously time-intensive and costly to change the shape of the A-pillar if it cannot be modified in the early development stage. For early determination of its shape, a reliable numerical methodology to predict vehicle interior noise due to the A-pillar vortex should be applied. This can be very challenging because the numerical method should simulate the complicated fluid behaviors as noise sources and the structural motions acting as transmission and propagation paths with acceptable precision. In this study, various numerical solvers are validated as the predictive tool of the interior transmitted noise in a simplified vehicle model. The solvers examined in the open benchmark study use various computational fluid and vibro-acoustic methods. It is shown that most of the software has prediction ability enough to industrial purposes.

Keywords: A-pillar vortex, aeroacoustic, benchmark I-INCE Classification of Subjects Number(s): 21.6

1. INTRODUCTION

The wind noise problem in commercial vehicles comes from three major types of noise, which are wind rush noise, leak noise, and cavity noise by reference (1). Wind rush noise can be produced by the interaction between a free stream and the vehicle's exterior shape, and this has broadband frequency characteristics. Pressure differences between vehicle surfaces and the interior volume can make many

1 munhcho@hyundai.com
2 hgun77@hyundai.com
3 dreamocs@hyundai.com
4 baramsolee@hyundai.com
5 ashok.khondge@ansys.com
6 fred.mendonca@cd-adapco.com
7 ljy@esi.co.kr
8 eschoi@exa.com
9 Bastien.Ganty@fft.be
10 raphael.hallez@siemens.com

auxiliary flows through small gaps, which generate leak noise with annoying noise region at high frequency bands. Cavity noise can be generated by the resonance between the flow movement and spatial geometry. Wind rush noise at the front seats contains the most energy of the interior transmission noise because free streams at high speeds are accelerated or interfered with, and interact with large extruding structures of the front upper body parts. Furthermore, the noise becomes more critical because the distance between the noise source and the passengers in the front seats are very close. In the front part of a conventional vehicle, most wind rush noise can be produced by an A-pillar vortex structure and complex wake structure behind outside rearview mirrors. In this study, we focus on the flow structure around the A-pillar region as the most important source of wind noise, in which flow can be accelerated by up to 60% of the free stream velocity and a very large vortex structure keeps rolling up, as shown in Figure 1 by reference (2).

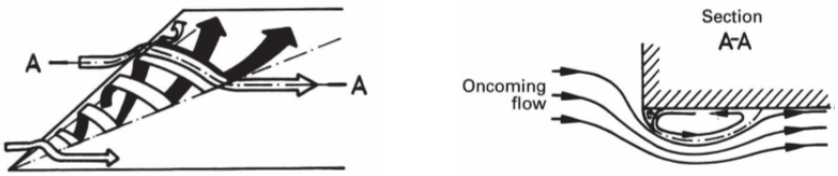

Figure 1 – A-Pillar vortex structure shown by reference (2)

The transfer mechanism of wind noise can be modeled as "source–transfer (transmission and propagation)–reception of noise". Noise sources can be produced by interactions between complex fluid structures and vehicle body shapes. Complicated waves and pressure fluctuations from unsteady fluid motion excite the surfaces of the window glass and body structures. Most of fluid vibrations will be transmitted through the window glass rather than the body structures because body structures contain complex hard materials and layers such as steel or aluminum panels, various sound absorption layers, and interior trims. Vibrations through glass can be propagated to passengers' ears, and the propagation should be affected by the acoustic characteristics of the interior cavity. This is the main reason that it is very difficult to reduce wind noise. To modify fluid structures on the exterior surfaces does not guarantee a reduction of the interior noise transmitted to passengers' ears. It means that not all aerodynamic motions are involved in interior noise generation. Some aerodynamic and aeroacoustic fluctuations on the glass surfaces would be amplified, while others would be diminished or blocked according to the characteristics of the transfer paths. Therefore, it is necessary to consider both transfer path characteristics and exterior wind noise sources for the reduction of flow-induced noise.

The reduction of noise induced by the A-pillar vortex should be considered in the very early stages of the vehicle development process, because the shape of the A-pillar is a crucial parameter in A-pillar vortex generation. It is very difficult to modify the noise level in the early stages without prototypes. Therefore, numerical methodology is required to the virtual verification and refinement of the flow-induced noise without actual test vehicles.

Interior noise generated by an A-pillar vortex can be modeled and simulated by the interdisciplinary study of computational fluid dynamics, aeroacoustics, and vibroacoustics. Numerical study of vibroacoustic systems excited by external aerodynamic and acoustic loads has been performed over many years. In particular, the fast improvement of high performance computing and numerical algorithms can guarantee greater accuracy in simulations for a greatly reduced calculation time. Hartmann et al. (3) conducted experimental and numerical studies for a simplified vehicle model based on SAE Type 4. The research provided very accurate experimental results, including surface sound pressures, noise transmission according to different types of glass, A-pillar shape and outside mirrors. Numerical studies of two commercial solvers were performed and validated. Through both experimental and numerical approaches, the details of noise sources could be analyzed through wavenumber-frequency decomposition.

In this study, the characteristics of the transfer path of interior noise by the A-pillar vortex will be studied through experimental approaches. Numerical simulations by several commercial software will be validated and compared to experimental results. This can show the ability and feasibility of applying numerical methodologies to the vehicle development process. The benchmark study can provide opportunities to improve the numerical accuracy of each solver. As a result, each solution maker can obtain a more accurate methodology or expertise as reported by reference (4).

2. Experimental Study

2.1 Simplified Vehicle Model

In order to reproduce strong vortical structures of the front upper part of a vehicle, an A-pillar vortex, which is a simplified vehicle model, was made for experimental and numerical studies. As shown in Figure 2, this model, which is called the Hyundai Simplified Model(HSM), can generate similar varied fluid structures to a commercial vehicle shape. It can make the front stagnation region, A-pillar vortex, separation, and reattachment regions of a roof's surface, and rear wake structures. Its exterior geometry is same as the previous benchmark study by Cho et al. (5) In particular, the model in this study has glass and an inner hollow space, as shown in Figure 3, which acts like a wind shield and door glass, interior sound absorption materials, and the interior cavity of a real vehicle. Its main body is made of aluminum panels (12t). The three float glass panes (1 windshield and 2 door glass) are 4mm thick. Sound absorption pads are attached to the inner surfaces of the cavity space. These pads are made of three layers, polyurethane layer (40t), a heavy layer (2t), and another polyurethane layer (20t). The absorption layers can show the effect of the actual interior material in a real road vehicle. Moreover, they can block structure-borne noise from transmitting from the aluminum body panels, and make most of the interior transmission noise transfer through the glass windows.

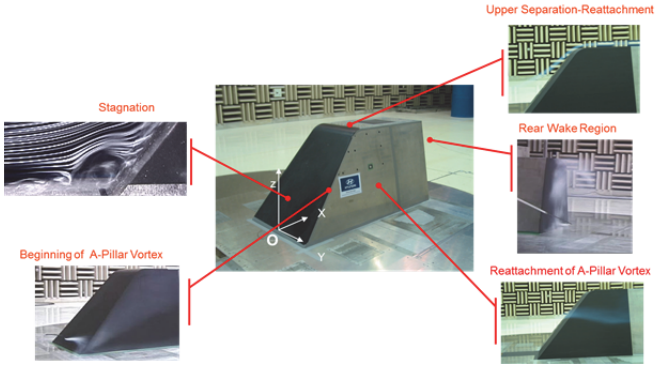

Figure 2 – Flow structures acound Hyundai Simplified Model (HSM)

Figure 3 – Hyundai Simplified Model for the study of interior transmission noise

2.2 Test Setup

Experimental processes were conducted for two objectives. One is to provide basic acoustic properties and characteristics for numerical studies; the other is to validate these numerical methodologies. First, we conducted frequency response function (FRF) tests to obtain the damping loss factor of each pane, the reverberation time tests of inner cavity space and several vibration tests were used to validate the boundary conditions of each pane and window frame. These results were given to all software solution makers for their numerical studies. The mechanical (density, Young's modulus, Poisson's ratio, etc.) and acoustic properties (Biot's parameters) of each material related to HSM were provided to all software makers. These are necessary in vibro-acoustic simulations such as finite element method (FEM), statistical energy analysis (SEA), or hybrid methods.

Second, in order to validate the numerical studies, the interior transmission noise was measured at Hyundai Aeroacoustic Wind Tunnel (HAWT), which is a closed circuit type wind tunnel with a maximum velocity of 200 km/h and a background noise level of 54 dBA at 100 km/h. As shown in Figure 4, two microphones were deployed to measure sound pressure. These were positioned asymmetrically, because of the binaural conditions of the driver's ears in a real road vehicle. Sound pressures were measured by high precision microphones (B&K 4189) at wind speeds of 110 and 130 km/h, and yaws of 0° and 10°.

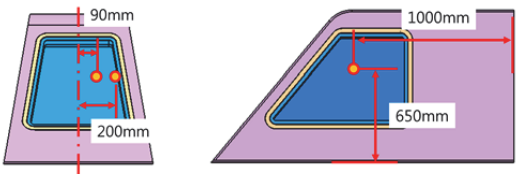

Figure 4 – Positions of the microphones in the inner cavity

2.3 Results and Analysis of Experiments

2.3.1 Characteristics of exterior aerodynamic excitation

At the beginning of sound generation, the exterior airflow structures around the HSM excited the transfer system of noise and vibration from fluid noise sources to inner noise perception points (the positions of the microphones). The measurement of static pressure on the side surface of the HSM is shown in Figure (5). It can be thought that the static pressure contours on the surfaces can represent the footprints of any large vortex structures. Figure 5(b) shows the vorticity magnitude on the side wall by particle image velocimetry (PIV) measurement. It can be found that airflow around the A-pillar has a strong swirling structure, known as an A-pillar vortex, and it is one of the largest structures generated by the interaction between free streams and HSM. The A-pillar vortex structure can keep its shape by flow separation at the leading edge of the pillar (Figure 5(b)) and reattachment on the side wall (Figure 5(a)). The reattachment angle is 25–30°.

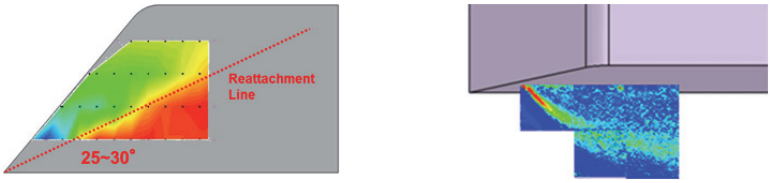

Figure 5 – Visualization of A-pillar vortex structure (left: Static pressures, right: Vorticity magnitude)

Sound pressure on the side surface could be measured to find the characteristics of the flow excitation by the A-pillar vortex as shown in Figure 6. Four points (P1–3, P7) among seven points are positioned in the A-pillar vortex. Figure 6(a) shows that fluid excitation becomes stronger closer to the reattachment line inside the vortex region, and the excitation becomes weaker outside this region. In Figure 6(b), several sound pressure profiles in the vortex can be simplified according to their frequency range. The acoustic excitation has broadband characteristics like “pink” noise, which has a particular frequency slope, f^{-1}. Acoustic excitation can be divided into three regions by frequency slopes. The first region corresponding to the $f^{-0.5}$ slope is positioned at 100–500 Hz, the second region of f^{-1} slope is in the range of 500–2000 Hz, and the last region consists of all excitations above 2000 Hz. The change of frequency slopes can show the lifecycle of substructures in the A-pillar vortex region. Large vortex substructures with low frequency movement are generated, advected, accelerated, and scattered; finally, small eddies with high frequency fluctuation become dissipated. Outside the A-pillar vortex region, such as P4, P5, and P6, the frequency slopes, which keep f^{-1} between 2000Hz and 4000Hz, are not so steep and the change in slope is much less than those inside the A-pillar vortex. This means that the fluid structure does not change dramatically as in the vortex, and weak pressure fluctuations are loaded onto the glass surface as a result.

(a) (b)

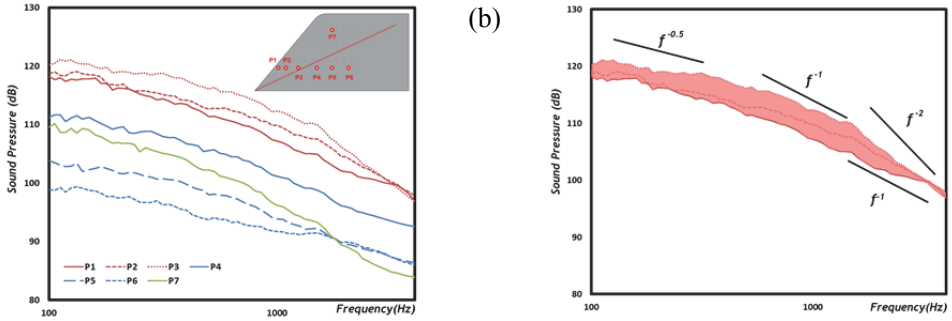

Figure 6 – Sound pressures on the side surface

2.3.2 **Characteristics of noise transmission path**

The transfer path from fluid excitation to interior noise reception points (two microphones) contain very complicated acoustic components such as glass transmission efficiency, glass modal behavior, glass boundary condition, interior absorption materials, and the acoustic characteristics of the inner cavity. The measurement of the noise transfer function can be very useful in figuring out the total characteristics of the transfer path. The impact excitation positions are shown in Figure 7, and the sound pressure response positions are shown in Figure 4. The transfer functions at each excitation point can be obtained as shown in Figures 8 and 9. At the upper region of the front and side glass windows (P2 and P3), transfer functions have several peaks between 150 Hz and 350 Hz. When the A-pillar vortex is generated and rolled up, the side walls are excited by broadband fluctuations, so it can be assumed that the shape of the transfer function can determine the frequency characteristics of the received sound pressure.

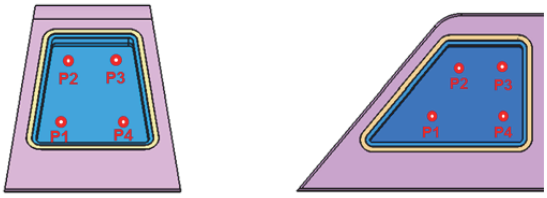

Figure 7 – Position of Accelerometers and Excitations at the front and side windows

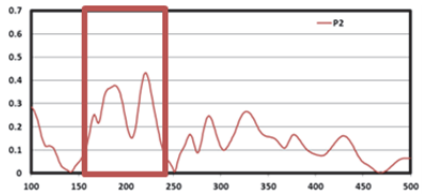

(a) TF of excitation at P2

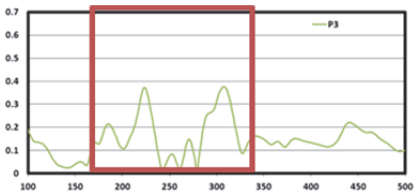

(b)TF of excitation P3

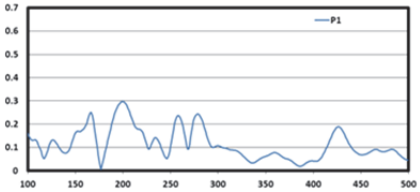

(c) TF of excitation at P1

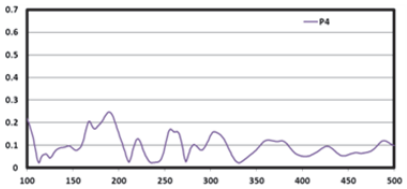

(d) TF of excitation at P4

Figure 8 – Transfer functions of the excitations (P1~P4) at the front window

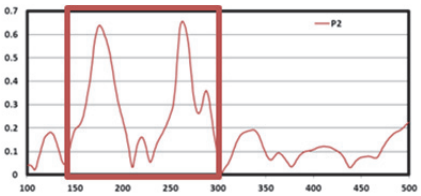

(a) TF of excitation at P2

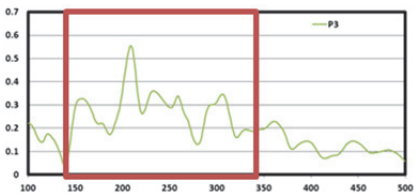

(b)TF of excitation P3

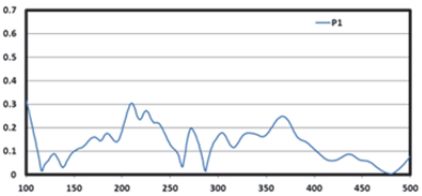

(c) TF of excitation at P1

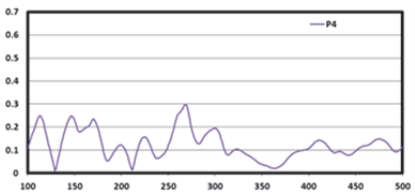

(d) TF of excitation at P4

Figure 9 – Transfer functions of the excitations (P1~P4) at the side window

2.3.3 **Verification of boundary condition of glass windows**

The effect of boundary conditions of glass windows should be validated for the analysis of noise transmission mechanisms and numerical modeling. It is very difficult to attach a glass panel to an aluminum window frame, because the simple and direct attachments between hard materials can make unnecessary leakage flows and fatigue cracks. Urethane spacers and silicon sealers are used in the gap between the glass and frame, as shown in Figure 10. The effect of the spacers and sealers can be verified through frequency response function (FRF) tests on the inside and outside of the frame surfaces. Figure 11 shows that the results of FRF test on both sides of the window frame are nearly the same. It can be thought that the boundary conditions of the sealers and spacers can be treated as a clamping condition or the simple attachment of two materials.

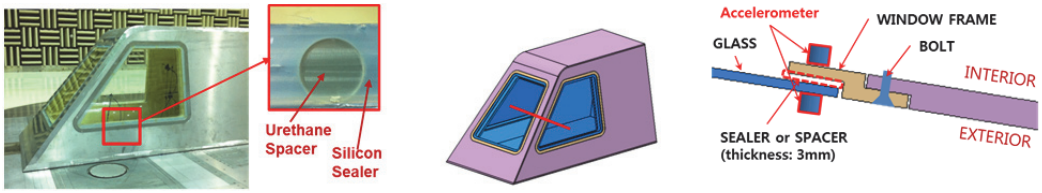

Figure 10 – Boundary conditions between the glass and the window frame

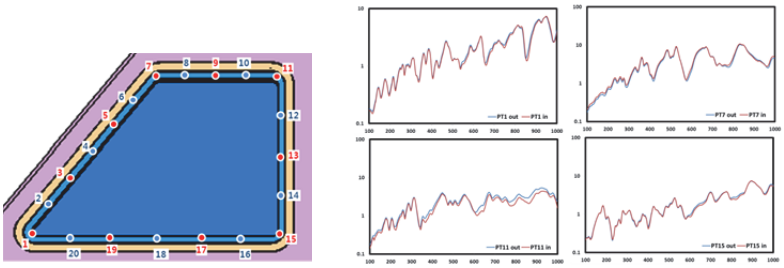

Figure 11 – FRF results of the inside and outside surfaces of the window frame

(red line: Inside measurement, blue line: Outside measurement)

2.3.4 **Analysis of interior sound pressure**

The results of sound pressure in the cavity are shown in Figure 12. It can be thought that the plot in the frequency domain can be divided into two regions; one region of between 100–500 Hz has a few peaky humps, and the other region of 500–4000 Hz has a flat shape with frequency slope, f^{-1}.

Figure 13 shows the noise transmission mechanism in the first region. The exterior aerodynamic excitation by A-pillar vortex has a broadband shape with a gentle slope, $f^{-0.5}$. Several peaks and humps can be found in the noise transfer function, and their positions are similar to those of the interior sound pressures. It can be found that the modal behaviors of the transfer path dominate the characteristics of noise transmission in the low frequency region.

The second frequency region is very different from the first. As shown in Figure 14, the slope of aerodynamic excitation by the A-pillar vortex within the 500–4000 Hz range, which is f^{-1}, is very similar to the slope of the interior sound pressure within the 500–4000 Hz range. In the region, the transfer function has a flat shape and a low quantity of responsibility. It can be said that the aerodynamic load that can be transmitted to the interior cavity keeps its frequency characteristics (the f^{-1} slope), but its fluctuating energy should be decreased through the transfer path. In the high frequency region, the movement of turbulent flows on the surfaces of HSM can determine the characteristics of the interior transmitted noise.

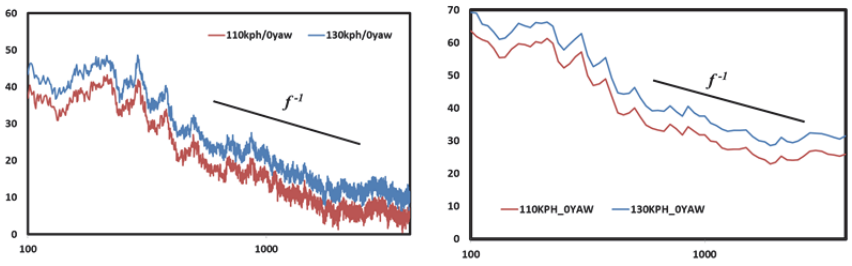

Figure 12 – sound pressures in the HSM cavity (left: Narrow band scale, right: 1/12 octave band scale)

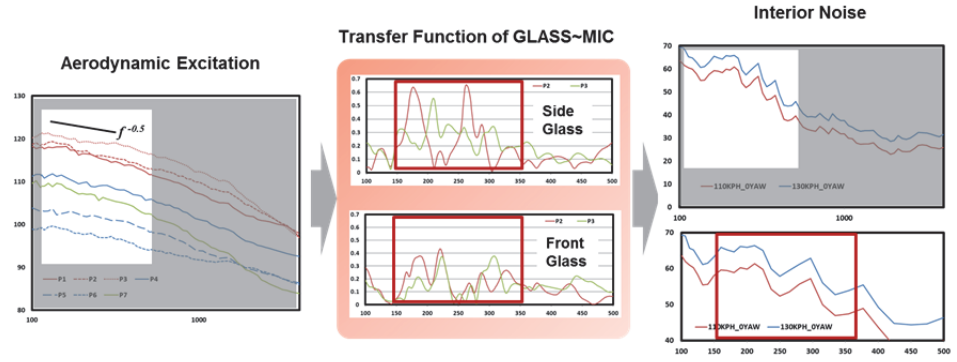

Figure 13 – Noise transmission mechanism (100Hz~500Hz)

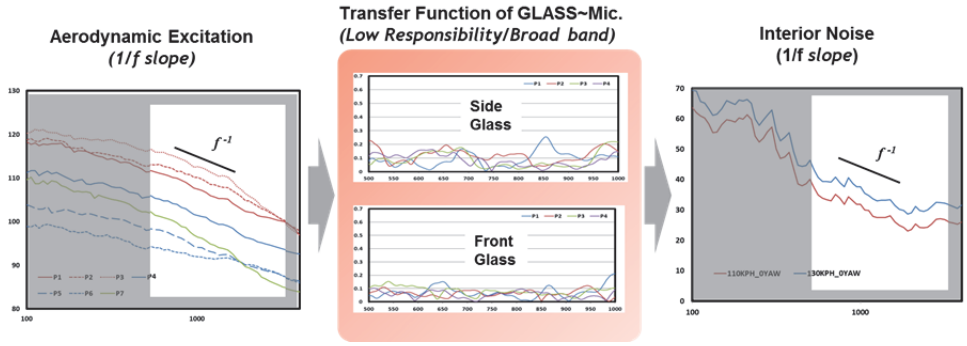

Figure 14 – Noise transmission mechanism (500Hz~4000Hz)

2.3.5 Visualization of noise sources

It can be concluded that the noise sources of the interior noise can be divided into the A-pillar vortex excitation in the low frequency region and the excitation by wall pressure fluctuation of turbulent flows in the high frequency region. This classification of noise sources can be validated by applying noise source visualization techniques. In this study, a beamforming method is applied to find the position of the noise sources. A portable beamforming device is positioned toward the side glass of the body of the HSM; Figure 15 shows the results of the noise source localization. The major sources in the low frequency range can be found at the vicinity of the A-pillar vortex, noise sources with high frequency behavior are distributed outside the A-pillar vortex region.

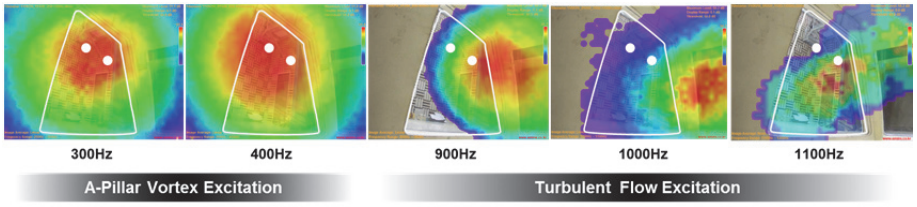

Figure 15 – Sound Visualization by Beamforming Method (white line: boundary of glass windows)

3. Results of Benchmark Study

3.1 Outline of Numerical Solvers

Various numerical solvers participated in the benchmark study, as shown in Table 1. No CAE solution makers have both a computational fluid dynamics (CFD) code and a vibroacoustic (VA) solver together. Solvers A, B, and C contain both type of solvers, but solvers D, E, and F do not. Solver D has a CFD code and solver F has VA codes, so they performed the cooperative numerical study. Solver E has only VA code, so it provided unsteady fluid data with a very high resolution with Solver A. In this integrated numerical study, no interfacial problems between different solvers occurred, and every solver could conduct a numerical study for the prediction of interior transmission noise with the best performance.

Table 1 – List of Commercial Numerical Solvers

	Solver A	Solver B	Solver C	Solver D	Solver E	Solver F
CFD solver	O	O	O	O	X *(with A)*	X *(with D)*
Numerical methods	LBM	FVM	FEM	FVM		
Turbulent model	VLES	iDDES k-ω-SST	LES Smagorinsky SGS	DDES-SST k-ω		
Time step	5.8e-6 s	2e-5 s	1.5e-5 s	2e-5 s		
Min. cell	1mm	2mm	1.5mm	0.05mm		
Mesh size	106M	55M	10M	55M		
VA solver	O	O	O	X *(with F)*	O	O
Numerical methods	SEA	*	FE-BEA & FE-SEA		FEM	FEMAO (Adaptive Order)
Mesh size (surface/ volume)	N/A	N/A	5,810/ 134,902		75,340/ 1,739,455	30,198 /168,026

* VA solution of solver B has been under development. So its detailed information cannot be opened before its official release.

3.2 Basic data for numerical study

All data necessary to the numerical study was provided before performing a simulation of each solver. The data contains experimental results and material properties to determine both the acoustic characteristics and the model geometries of HSM and test conditions.

Reverberation tests were conducted to find the reverberation time in the cavity space, as shown in Figure 16(a). FRF tests at the glass surfaces and window frames were performed to configure the damping loss factors and boundary conditions for any of the numerical solvers. The acoustic and mechanical properties of each HSM material were suggested, which includes their transmission loss in Figure 16(b), Young's modulus, Poisson ratio, density and Biot's parameters.

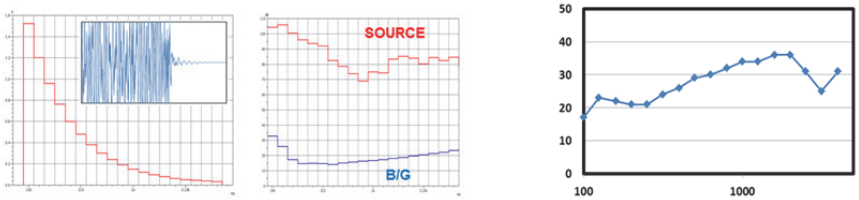

(a) Reverberation Time (b) Transmission loss

Figure 16 – Acoustic parameters for numerical study

3.3 Validation Study of Numerical Solvers

A comparison between the experimental results and the numerical studies is shown in Figure 17. All numerical and experimental results are presented at the 1/3 octave band. The simulation results are updated with the latest modified version for each solver. Solver A, B, and C have both CFD and VA solutions. The validation results show that the integrated solvers were very successful. Solver A and B follow the tendencies of experimental results with good precision in the 100–4000 Hz range. Solver C does not predict well at frequencies less than 300 Hz; it would require modification by different approaches of FEM modeling. Cooperation between different solvers could achieve better accuracy than expected. Solvers D and F performed simulations with good precision in each area of

CFD and VA; their combined work could give very accurate results, because they already have experience of partnership. Even though the integrated work of solvers E and A in this study was their first trial, their cooperation worked very well when they were able to overcome small problems of data interfaces. Both the integrated solution of a single solver and cooperation between different solvers can guarantee reliable numerical result applicable to the actual development process.

In the driving conditions of an actual vehicle, drivers and passengers receive interior noises with two ears. In this study, sound pressures were measured at two asymmetric points in order to validate their ability to capture the binaural condition shown in Figure 4. Figure 18 shows the difference of sound pressures at two points of the experimental and numerical results. Solver A cannot show binaural results, because of the limits of its VA application based on statistical energy analysis (SEA). In the case of solver C, the binaural effect cannot be shown in frequency ranges of more than 1 kHz, because it applied an FE-SEA method in that range. On the other hand, FEM-based solutions can predict binaural effects with acceptable accuracy. It can be said that the simulation of binaural effects in the vehicle cabin is not necessary for the application of numerical methodologies in early stages of the industrial development. If sound quality design is required in advanced processes, the binaural effect should be simulated and analyzed for acoustic load balancing in the cabin.

Through this benchmark study, all solution makers can obtain technical knowledge and experience for more precise simulation. Some solvers were able to achieve better accuracy in their results after their second or subsequent trials. It can be found that it is very important to simulate every step of varying physical phenomena for the highest precision. Figure 19(a) shows the critical discrepancy between experiments and simulated data in the first simulation, which were made by solver E and another CFD solver (not solver A in the first simulation). This resulted from insufficient resources being used in the flow simulation, which generated some errors. The discrepancy could be dramatically reduced by applying the CFD results of solver A. Accuracy in CFD study determines the total accuracy of the numerical study, even if the VA methodology was perfect. Figure 19(b) shows that the improvement of numerical results can only be achieved by modifying the damping effect in the transmission system. The modification of CFD and VA parts makes a small improvement in the numerical results in Figure 19(c). The modification examples shown in Figure 19 conclude that the total accuracy of any numerical study should be dominated by the numerical step with the worst accuracy.

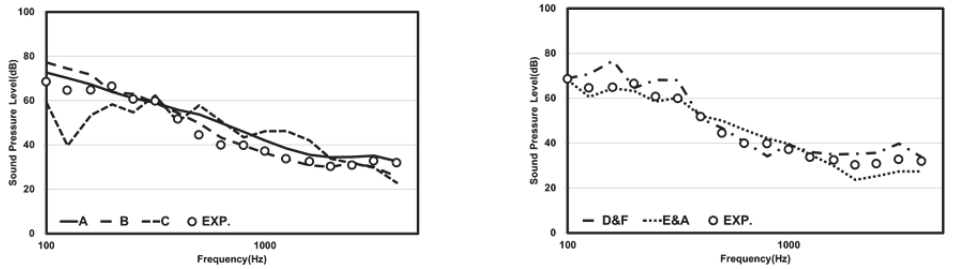

(a) Wind speed at 110 km/h and yaw angle at 0°

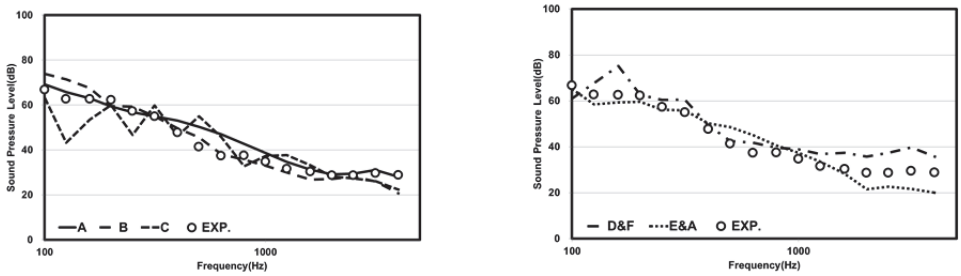

(b) Wind speed at 110 km/h and yaw angle at 10°

Figure 17 – Comparison of interior sound pressures by simulations and experiments

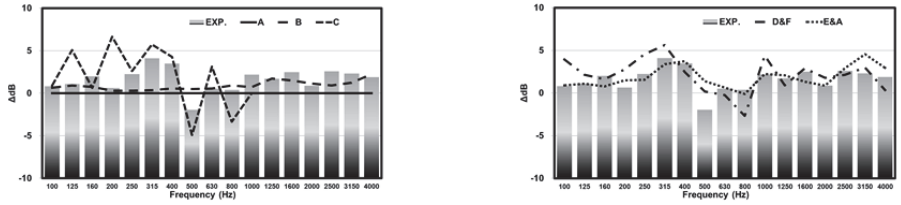

(a) Wind speed at 110 km/h and yaw angle at 0°

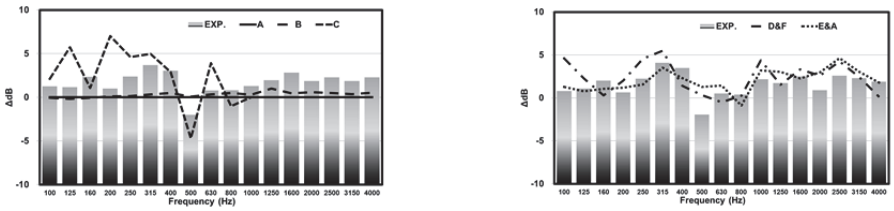

(b) Wind speed at 110 km/h and yaw angle at 10°

Figure 18 – Comparison of binaural effect obtained by simulations and experiments

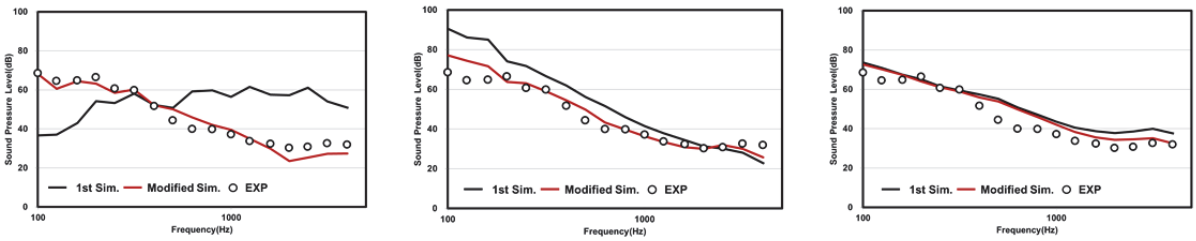

(a) Solver E (b) Solver B (c) Solver A

Figure 19 – Examples in modification of some numerical solvers

4. CONCLUSIONS

Wind noise is essentially an integrated phenomenon of different physics systems such as fluid dynamics, aeroacoustics, and vibroacoustics. This study shows that the complicated phenomenon of wind noise transmission can be simulated by several numerical solvers. Various types of numerical solvers were used in the benchmark study, and their applicability in the vehicle development process was demonstrated. Some solvers have both CFD and VA solutions, and others do not. The integrated solution of CFD and VA could be used to prove the numerical reliability of the software packages. If the data interface problem can be solved, the cooperation of different solvers could guarantee the high precision of results. The solution makers attending the benchmark test can obtain varied knowledge that would allow them to apply their solutions to actual wind noise problems. Each solver tried to perform modified simulations several times. Some solvers were able to achieve higher accuracy results and got the opportunity to determine their own strengths and weaknesses.

ACKNOWLEDGEMENTS

The authors would like to thank ANSYS, CD-adapco, ESI, Exa, Free Field Technology, MSC and Siemens PLM (listed in alphabetical order) for their technical supports and advices.

REFERENCES

1. Callister JR, George AR. Wind noise. In: Hucho W editor. Aerodynamics of road vehicles. 4th ed. Warrendale: Society of Automotive Engineers, Inc.; 1998, p.343-364.
2. Watanabe M, Haruta M, Hayashi E. The effect of body shapes on wind noise. SAE Paper No. 780266, 1978.
3. Hartmann M, Ocker J, Lemke T, et al. Wind Noise caused the A-pillar and the Side Mirror Flow of a Generic Vehicle Model. Proc 18th AIAA/CEAS Aeroacoustics Conference; Colorado Springs, USA 2012.
4. Mendonca F, Connelly T, Bonthu S, Shorter P. CAE-Based Prediction of Aero-Vibro-Acoustic Interior Noise Transmission for a Simple Test Vehicle. SAE Technical Paper 2014-01-0592, 2014
5. Cho M, Oh C, Kim HG, et al. Benchmark Study of Commercial CFD Solvers for Sunroof Buffeting in a Simplified Vehicle Model. Proc INTER-NOISE 2013; 15-18 September 2013; Innsbruck, Austria 2013.